Computational assessment of transport distances in living skeletal muscle fibers studied in situ

Kenth-Arne Hansson[1,2], Andreas Våvang Solbrå[1, 2, 4] , Kristian Gundersen[1,2,] and Jo Christiansen Bruusgaard[1,2,3, §]

[1]Department of Biosciences, University of Oslo, Oslo, Norway

[2]Center for Integrative Neuroplasticity, Department of Biosciences, University of Oslo, Oslo Norway

[3]Department of Health Sciences, Kristiania University College, Oslo, Norway

[4]Department of Physics, University of Oslo, Oslo, Norway

[§]Corresponding author

Abstract

Transport distances in skeletal muscle fibers are mitigated by these cells having multiple nuclei. We have studied mouse living muscle fibers in situ and determined cellular dimensions and the positions of all the nuclei within fiber segments. We modelled the effect of placing nuclei optimally and randomly using a nucleus as an origin of a transportation network. It appeared that an equidistant positioning of nuclei minimizes transport distances along the surface for both muscles. In the soleus muscle however, which were richer in nuclei, positioning of nuclei to reduce transport distance to the cytoplasm were of less importance, and these fibers exhibit a pattern not statistically different from a random positioning of nuclei. Together, these results highlight the importance of spatially distribute nuclei to minimize transport distances to the surface when nuclear density low, while statistically it appears that the distribution are of less importance at higher nuclear densities.

Introduction

The largest cells in the vertebrate body are the muscle fibers and their vast size introduce logistical problems with respect to synthetic capacity and transport of macromolecules. For example, a human sartorius muscle have an average fiber length of 42 cm (Sandve *et al.*, 2011) and a fiber cross sectional area of about 2500 μm^2 (Kann, 1957). This leads to a volume of 1050 nl, more than 4000 times the volume of the cell that is most often mentioned as the largest cell in the body; the human egg. Most other mononucleated cells range 5-20 µm in diameter and, assuming a spherical shape, have volumes less than 0.004 nl. The cell body of an alpha motor neuron might have a diameter of 50 µm and assuming a spherical shape this gives a volume of about 0.07 nl. In addition, it might have an axon spanning 1 m, and with a diameter of 7 µm this yields a volume of 38 nl. The motor neuron might thus be the second largest cell type in a human body, albeit the sartorius cell still has a volume almost 30 times larger. Smaller muscles might have cells with volumes more similar to the motor neurons.

When cells become larger, the average transport distances increase and thus influence the overall transport times. Hence, small and large cells operate under different time scales (Cadart *et al.*, 2019). In larger cells, molecules would acquire longer transport times to reach their target. Because diffusion times, t, scale to the distance travelled L as $t \propto L^2$, diffusion is more efficient at shorter distances. In contrast, active transport times scale linearly to the distance travelled, although the

speed relies heavily upon the molecular kinetics of the motor proteins. Typically, a kinesin motor moves at a speed of 1μm/s along the microtubules (Pilling *et al.*, 2006), while the myosin V moves at 3μm/s on the actin filaments (Schott *et al.*, 2002).

Mammalian skeletal muscle cells are syncytia, and human muscle cells typically have myonuclei distributed along the fiber at a density of about 100 per mm length (Cristea *et al.*, 2010), thus a sartorius muscle cell might have more than 40 000 nuclei. The high number of nuclei is believed to be necessary due to the vast cytoplasmic volumes and long transport distances, and both the positioning and the number of nuclei seems to be regulated to overcome these challenges (Bruusgaard *et al.*, 2003; Bruusgaard *et al.*, 2006; Metzger *et al.*, 2012b; Gundersen, 2016). We have previously suggested that the myonuclei seems to be distributed as if to repel each other to minimize cytoplasmic transport distances (Bruusgaard *et al.*, 2003; Bruusgaard *et al.*, 2006). This optimization seems to be important since perturbation of the nuclear positioning has been reported to impair muscle function (Metzger *et al.*, 2012a; Folker & Baylies, 2013).

The fact that these cells are multinucleated has led to the proposal of a so-called cytoplasmic-to-nucleus domain that signifies a theoretical cytoplasmic domain governed by a single nucleus (Strassburger, 1893). Each nucleus is surrounded by a synthetic machinery that seems to remain localized (Pavlath *et al.*, 1989; Mishra *et al.*, 2015), and it has been shown that some proteins are localized in the vicinity of

66 the site of expression both in vitro (Hall & Ralston, 1989; Pavlath *et al.*, 1989; Ralston
67 & Hall, 1992a) and in vivo (Merlie & Sanes, 1985; Sanes *et al.*, 1991).

68 In hybrid myotubes in which one or a few nuclei were derived from myoblasts
69 expressing non-muscle proteins it was found that mRNAs for nuclear, cytoplasmic
70 and ER-targeted proteins, had similar distributions, and were in most cases confined
71 to distances 25-100 µm from the nuclei (Ralston & Hall, 1992b). Similar observations
72 were made with virus infected isolated muscle fibers in culture, with the additional
73 observation that virus coded mRNA did not venture into the fiber interior but
74 remained around the nucleus at the fiber surface at least for the first 40 hours after
75 infection (Nevalainen *et al.*, 2013). These and other observations support the notion
76 that myonuclei support the expression of different genes within a
77 compartmentalized region of a fiber (Cheek, 1985; Hall & Ralston, 1989; Pavlath *et*
78 *al.*, 1989). The most prominent example is the acetylcholine receptor that is
79 normally expressed only in the nuclei near the endplate, and expression outside this
80 area (acetylcholine super-sensitivity) seems to require that the receptor is
81 transcribed in nuclei along the entire length of the fiber (Merlie *et al.*, 1984;
82 Gundersen & Merlie, 1993).

83 On the other hand, experiments where aggregated blastomeres from two different
84 mouse strains expressing distinct forms of cytosolic metabolic enzymes display,
85 heterodimers of the enzyme in the syncytial muscle tissue (Mintz & Baker, 1967) and
86 histological examination displayed no mosaicism in the cellular distribution of the

87 enzyme variants in muscle fibers (Frair & Peterson, 1983). This means that some
88 smaller proteins that are not trapped in structures such as synapses and sarcomeres
89 can be distributed over longer distances, and that the nucleus of origin is of less
90 importance.

91 To get a better understanding how nuclear positioning may affect transport
92 distances in muscle fibers we employed precise confocal imaging and 3D
93 reconstruction of fibers labelled in vivo in the soleus and EDL muscle. These muscles
94 differ in their myonuclear density and their nuclear distribution (Bruusgaard *et al.*,
95 2003), and thus potentially highlight variations in nuclear pattern due to differences
96 in functional needs and composition of the interior. We therefore modelled a
97 nucleus' as an origin of transportation network, and derived the area and volume of
98 responsibility by Voronoi segmentation (Du *et al.*, 2010) as well as transport
99 distances to the surface and cytoplasm. Additionally, we used simulations of
100 transport distances to analyze the energy trade-off by letting a protein diffuse locally
101 from a nucleus or being actively transport to parts of the fiber.

102 # Results

103 We have analyzed fiber segments of live surface fibers of EDL and soleus muscle in
104 situ. Nuclei were generally confined to the fiber surface, hence we analyzed nuclear
105 domains both in 2D (as surface domains along the sarcolemma) and in 3D (as volume
106 domains of the fiber cytoplasm).

107 **Cross sectional area and nuclear number in individual muscle fibers from the**
108 **EDL and soleus muscle**

109 Quantification of nuclear number after injecting fluorescently labelled
110 oligonucleotides, and fluorescent dextran (Fig. 1A), revealed that the EDL fibers had
111 approximately twice as many nuclei (47±10 nuclei /mm) compared to the soleus
112 fibers (88±29 nuclei/mm). Reconstructions of fiber segments from confocal stacks
113 (Fig. 1C and D) showed that the EDL fibers were about 31% larger than those in the
114 soleus (Fig. 1F). On average, the EDL muscle had a CSA of 1091± 278.4 μm^2 and the
115 soleus 831.8± 241.3 μm^2. These differences in nuclear number and size resulted in
116 EDL fibers having volume domains 130% larger than soleus fibers (Fig. 1G), and 93%
117 larger surface domains than in the soleus (Fig. 1H). The domain volumes in the EDL
118 were on average 23468 ± 5930 μm^3 and 10187 ± 3432 μm^3 in the EDL and soleus
119 muscle, respectively. In the EDL, surface domains were on average 2907 ± 582 μm^2,
120 while in the soleus they were on average 1508 ± 582 μm^2.

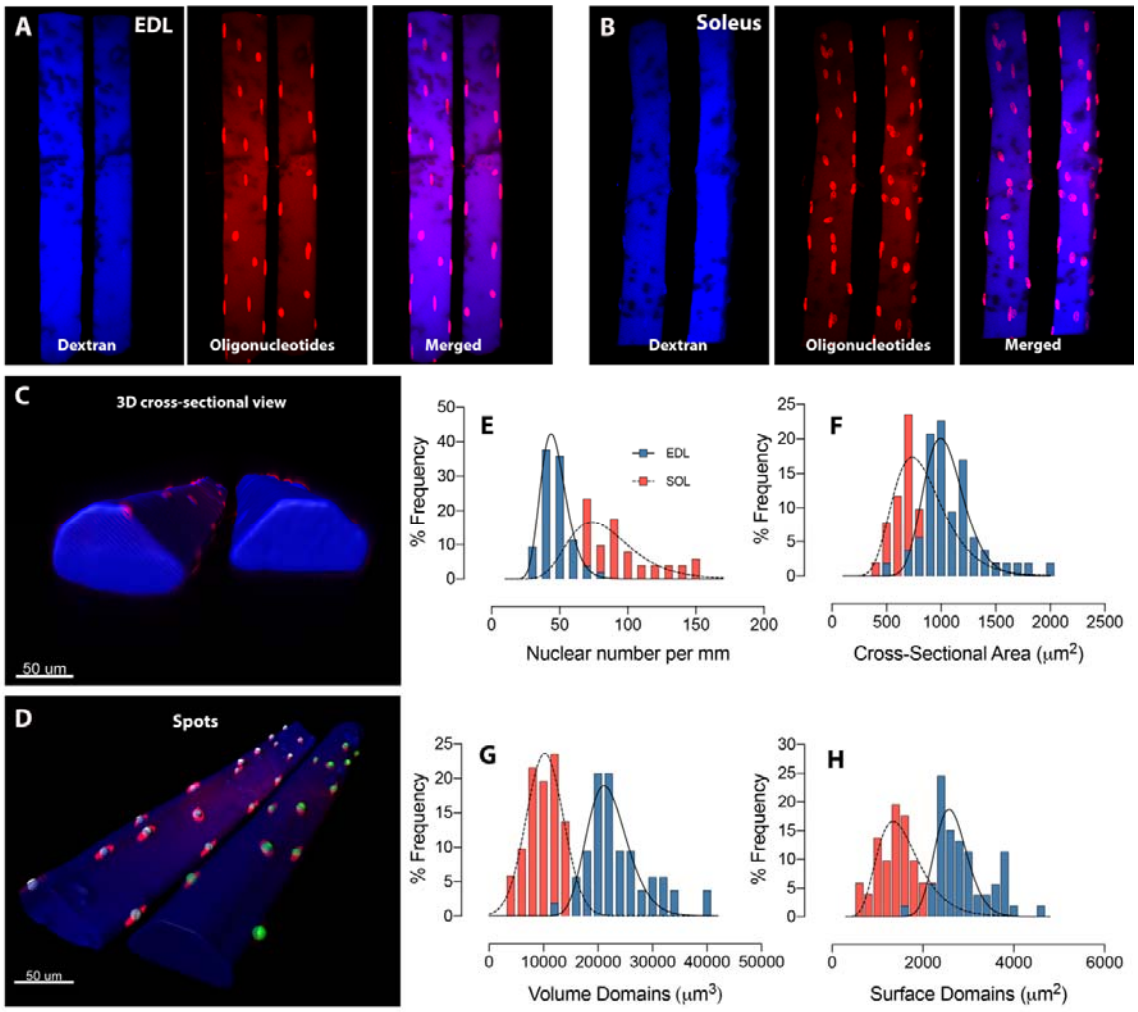

Figure. 1. Three-dimensional modeling of muscle fibers after in vivo injections and confocal imaging. (A) Representative collapsed z-stacks of fibers from the EDL and (B) soleus muscles, injected with dextran (blue) and labelled oligonucleotides (red). (C) Fibers 3D modelled based on the fluorescence from the cytosolic dextran. (D) Example of automatic assignment of spots to each myonucleus in order to define their 3D coordinates for subsequent analysis. (E) Frequency distribution of nuclear number and (F) cross sectional area, domain volume (G) and surface domains (H) in the EDL (blue) and soleus muscle (red).

129 **EDL and soleus display pattern differences of their domains**

130 While the average nuclear domains are a simple function of the density of nuclei,
131 and independent of how the nuclei are distributed, our data allowed us to study the
132 distribution of the individual myonuclear domains. In a nuclear distribution where
133 the distance between the nuclei is optimized, all domains would in principle be of
134 equal size. Any deviation from that would imply a non-optimized positioning of
135 nuclei, which may indicate that some domains would be unnecessary large and
136 represent "lacuna" where transport distances might be rather long.

137 To analyze how individual surface domains is influenced by the distribution of nuclei,
138 we performed a detailed quantification of individual nuclear domains for each
139 nucleus. Voronoi segmentation is a common way of formally quantifying areas or
140 volumes of "influence" for distributed entities of the same kind. We modelled
141 individual Voronoi domains by partitioning the fiber into sub-compartmentalized
142 surface areas (Fig. 2A) and volumes (Fig. 3A) based on the position of each individual
143 nucleus. To compare differences between nuclear distributions in the two muscles
144 we used the standard deviation of the domain sizes. In EDL the observed values for
145 the standard deviation measured for the Voronoi areas were not too different from
146 those obtained when the nuclei were placed optimally, but some fibers showed
147 much larger variability (Fig. 2B), indicating a less optimal distribution with some large
148 lacunar domains. In the soleus, however, the observed pattern resembled more the
149 values obtained when nuclei were placed randomly on the fiber surface (Fig. 2D).

150 There was no obvious difference in the variation of nuclear patterning with fiber size

151 (Fig. 2C and E).

152 Statistically, domain areas of the observed distribution were different from a

153 random positioning of nuclei (mean difference in the SD of 641μm^2; $p<0.0001$ in the

154 EDL and 194μm^2; $p<0.0001$ in the soleus) as well as optimal positioning (mean

155 difference in the SD of , 405μm^2; $p<0.0001$ for the EDL, and 432μm^2; $p<0.0001$ for

156 the soleus).

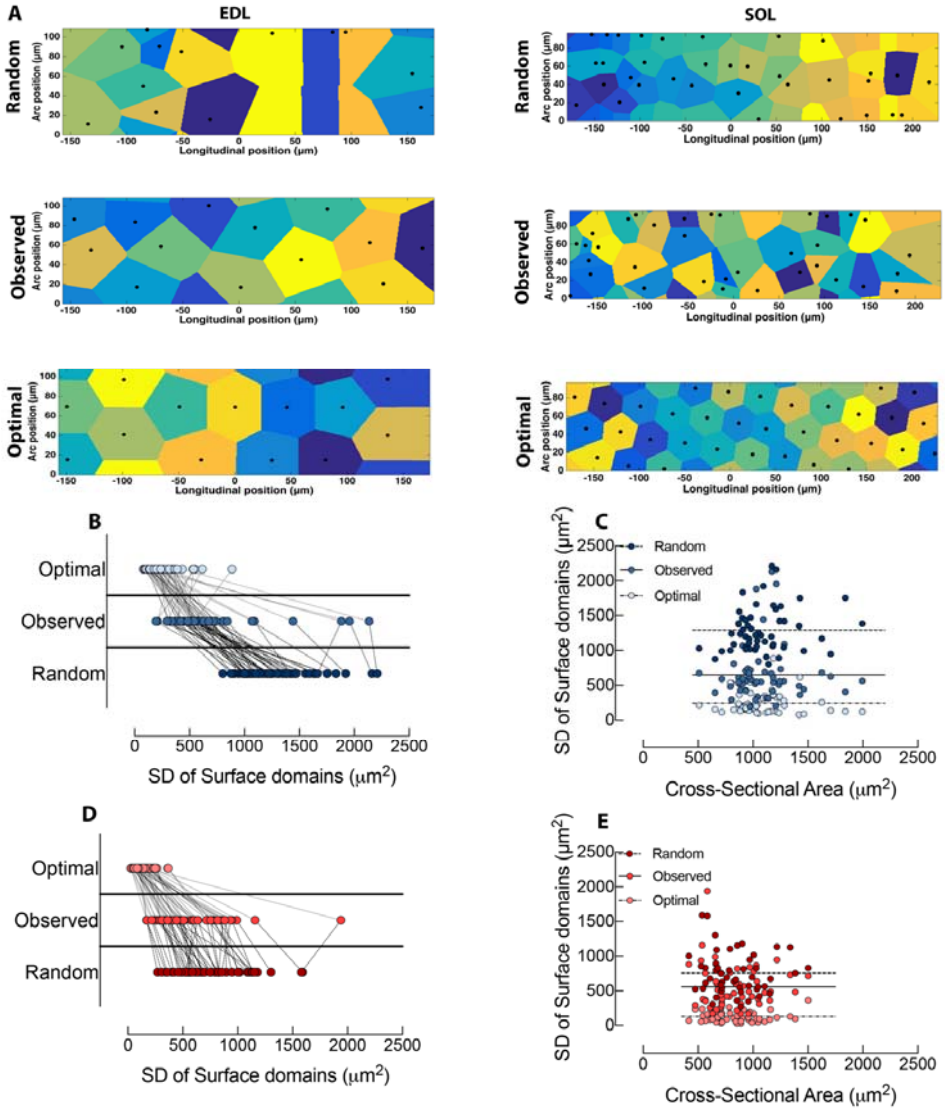

Figure 2. EDL and soleus display differences in patterning of Voronoi areas. (A) Representative Voronoi diagrams of individual domain areas in fibers from the EDL and soleus in the observed distribution and where nuclei were placed randomly or optimally on the fiber surface. (B) Comparison of observed and simulated nuclear patterns in the EDL muscle and (D) soleus plotted as a nested connection between the variation (standard deviation) of individual domains within a single fiber. Dashed and dotted lines signify the inter-specific connection between standardized variation of random-observed and observed-optimal. (C) Variation of surface domains plotted against the cross-sectional area in the EDL and (E) soleus. The relationship between variation and cross-sectional area was non-significant: Random (EDL, p=0.1625; SOL, p=0.5160), observed (EDL, p=0.8844; SOL, p=0.5858) and optimal (EDL, p=0.6892; SOL, p=0.9167).

167 Next, we analyzed the Voronoi volumes (Fig. 3A), the difference between the two
168 muscles resembled the values obtained when comparing Voronoi areas. Thus, in the
169 EDL the variability resembled an optimal distribution (Fig. 3B), whereas in the soleus
170 the variability was closer to placing the nuclei randomly (Fig. 3D). There was no clear
171 effect of fiber size on the variation on Voronoi volumes (Fig. 3C and E).

172 Statistically, domain volumes of the observed distribution were different from a
173 random positioning of nuclei (mean difference, 6521μm^3; $p<0.0001$ in the EDL and
174 mean difference, 224μm^3; $p<0.0001$ in the soleus) as well as optimal positioning
175 (mean difference, 6306μm^3; $p<0.0001$ for the EDL, and 4084μm^3; $p<0.0001$ for the
176 soleus).

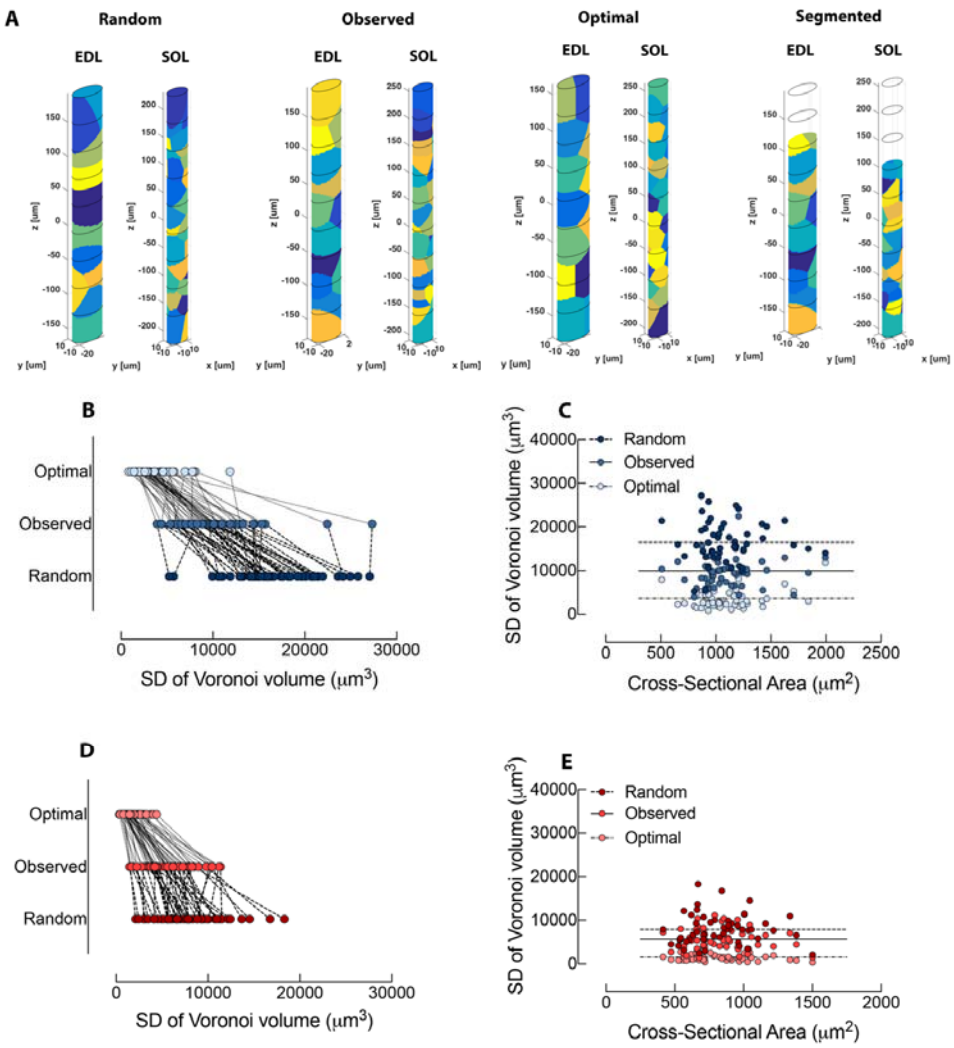

Figure 3. EDL and soleus display differences in patterning of Voronoi volumes. (A) Representative Voronoi diagrams of individual domain volumes in fibers from the EDL and soleus in the observed distribution and where nuclei were placed randomly or optimally on the fiber surface. (B) Comparison of observed and simulated nuclear patterns in the EDL muscle and (D) soleus plotted as a nested connection between the variation (standard deviation) of individual domains within a single fiber. Dashed and dotted lines signify the inter-specific connection between standardized variation of random-observed and observed-optimal. (C) Variation of surface domains plotted against the cross-sectional area in the EDL and (E) soleus. The relationship between variation and cross-sectional area was non-significant: Random (EDL, p=0.9651; SOL, p=0.9965), observed (EDL, p=0.9843; SOL, p=0.8789) and optimal (EDL, p=0.0627; SOL, p=0.4078).

187 **Transport distances vary between the EDL and soleus muscle**

188 The perhaps most relevant measure for judging the importance of nuclear density
189 and positioning is the actual transport distances along the surface or through the
190 cytoplasm. To model this, a grid of points corresponding to the pixel size was placed
191 on the surface or in the volume of each fiber. The closest distance from these points
192 to the nearest nuclei was calculated both on the surface (Fig. 4A) and in the fiber
193 volume (Fig. 5A).

194 Comparing transport distances along the surface between different nuclear
195 distributions showed that on average, EDL fibers had transport distances (23± 4.7
196 µm) 10% larger compared to the value obtained by placing nuclei optimally (21± 2.5
197 µm). When nuclei were placed randomly (27± 3.2 µm), the average distance were
198 increased by 29% relative to optimal distances and the observed distances were
199 closer to an optimal distribution (Figure 4B). In the soleus muscle, fibers had
200 transport distances (20±9.2 µm) 25% larger compared to the average transport
201 distance when nuclei were placed optimally (16±4.2 µm), while placing nuclei
202 randomly (20±5.5 µm) was essentially identical to the observed distances (Fig. 4C).

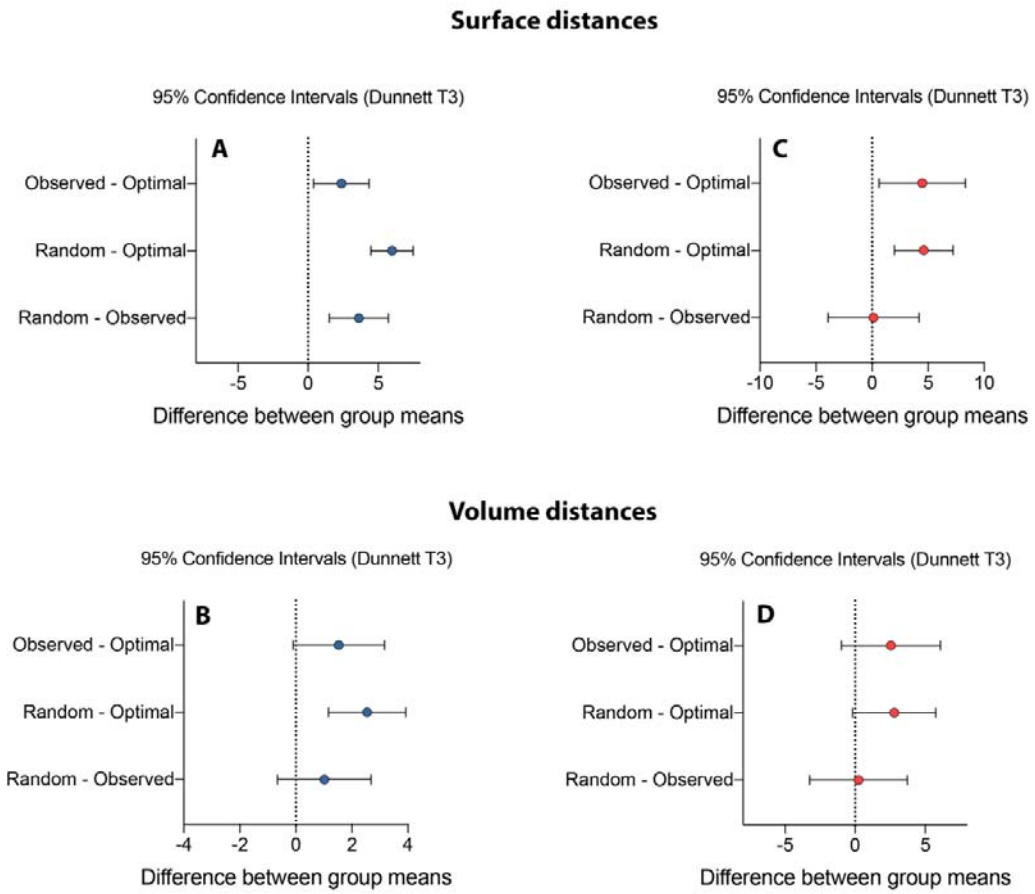

Supplementary figure 1. A groupwise Brown-Forsythe analysis of differences of transport distances along the surface (EDL, A; SOL, C) and cytoplasm (EDL, B; SOL, D). For all graphs, 95% confidence intervals overlapping a zero difference between means is regarded as non-significant comparisons. A Dunnett post hoc test were performed to correct for multiple comparisons.

For average transport distances in the cytoplasm (Fig. 5B), the observed distances in the EDL (22±3.6 µm) were closer to those seen when nuclei were placed randomly (23±2.7 µm) compared to nuclei placed optimally (21±2.6 µm). Interestingly, distances to the cytoplasm retrieved from placing nuclei randomly (20±5.5 µm) or optimally (17±5.7 µm) in the soleus (Fig. 5C) were not significantly different from

213 observed transport distances (20±7.5µm). In the EDL, there was a statistical
214 improvement in placing nuclei optimally compared to the observed and random
215 transport distances to the surface, and in the cytoplasm (Supp. Fig. 1A, B). However,
216 there was no statistical difference between observed placement of nuclei and its
217 transport distances to the cytoplasm when compared to optimal and randomly
218 positioned nuclei (Supp. Fig.1B). In fibers of the soleus muscle, there was a statistical
219 improvement when placing nuclei optimally for transport distances along the surface
220 (Supp. Fig. 1C), but no improvement within the cytoplasm (Supp. Fig. 1D).

221 The average transport distance might not reflect whether there are some areas or
222 volumes that is far away from any given nucleus, giving rise to lacunas that might
223 have an insufficient supply of macromolecules. Therefore, we analyzed the distances
224 on a per nucleus basis. Distribution of individual nuclear distances were fitted with a
225 Gaussian function (Fig. 4D, E and Fig. 5D, E). It was evident from the Gaussian fit that
226 the actual transport distances along the surface in the EDL where much improved
227 compared to a random distribution and was approximating an optimal distribution
228 (Fig. 4D). Similar conclusions were obtained analyzing optimal transport distances in
229 the cytoplasm. Notably the longer transport distances were less prevalent by the
230 natural placement of nuclei compared to a random distribution.

231 Soleus displayed similar traits when the transport distances along the surface (Fig.
232 4E) and cytoplasm (Fig. 5E) was analyzed, but the observed distribution was more
233 similar to a random distribution.

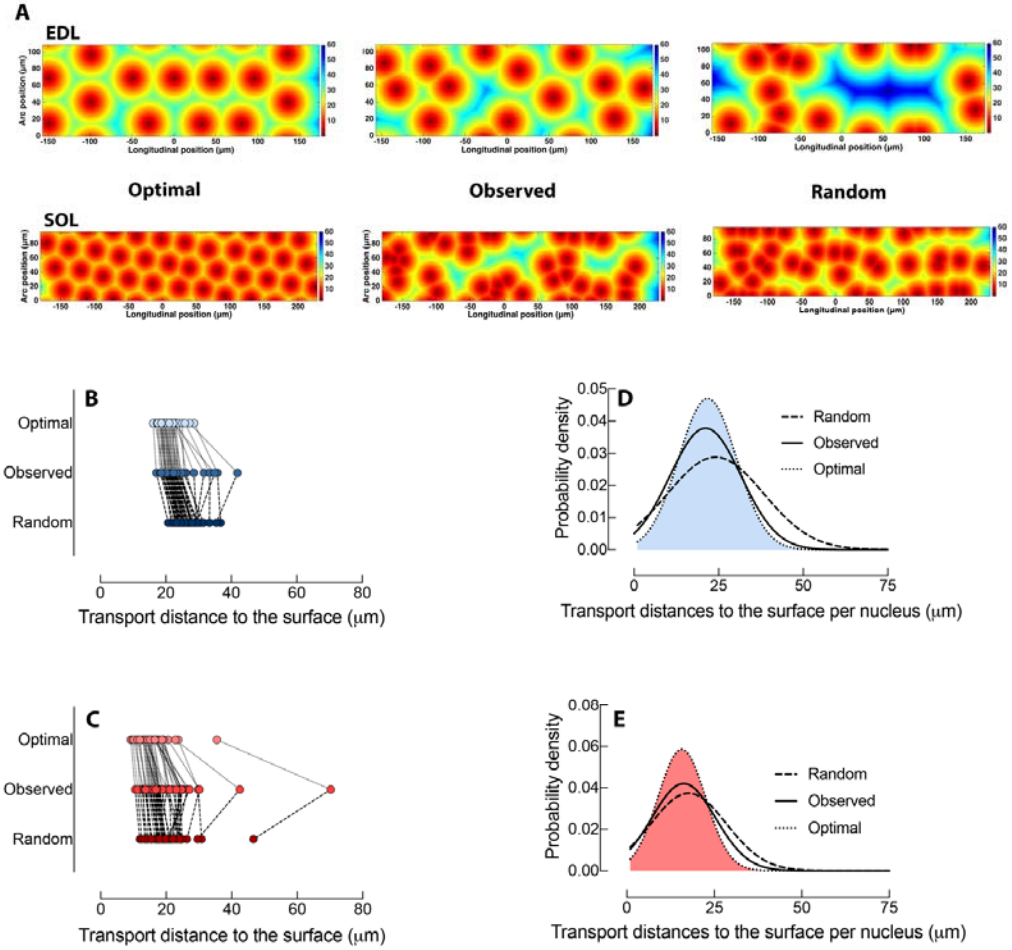

Figure 4. Quantitated measurements of transport distances along the fiber surface. (A) Fiber surface distance maps of fibers in the observed distribution and where nuclei were placed randomly or optimally on the fiber surface. (B-E) the average surface distance to the nearest nucleus were calculated and compared with observed transport distance. (B) Transport distances in the EDL muscle (blue) compared by their mean value per fiber, and per nucleus after a Gaussian fit (D). (C) Transport distances in the soleus muscle (red) compared by their mean value per fiber and per nucleus after a Gaussian fit (E). Dashed and dotted lines in (B and C) signifies the inter-specific connection between random-observed and observed-optimal. The Red-Green-Blue (RGB) vertical scale bar/ color gradient in (A) signifies the distance at 0μm-30μm -60μm from its nuclear origin.

243 In the EDL we found that 37% of the surface was longer than 25µm from the nearest

244 nucleus, compared to 28% when nuclei were placed optimally and 47% randomly. In

245 the soleus 27% of the fiber surface were longer than 25 µm from the nearest nucleus

246 in the observed distribution, compared to 8% and 23% in the optimal and random

247 distribution, respectively. Interestingly, and despite differences in fiber size and

248 nuclear number, both muscles displayed about 97% of their surface to be within 50

249 µm of its nearest nucleus (Table I)

250

TABLE I. Percent of the cytosol or surface to its nearest nucleus at different distances

	Distance (µm)	Observed (%)		Optimal (%)		Random (%)	
		EDL	Soleus	EDL	Soleus	EDL	Soleus
Surface	0-25	63	77	72	92	53	73
	25-50	34	20	28	7	41	25
	> 50	3	3	0	1	6	2
Cytosol	0-25	69	79	77	88	62	77
	25-50	30	18	23	11	36	22
	> 50	1	3	1	1	2	1

251

252 In terms of volumes, 31% of the cytoplasm in the EDL were longer then 25 µm from

253 its nearest nucleus during observed distributions, increasing to 38 % when nuclei

254 were placed randomly, and 23% with optimal distribution of the nuclei. The soleus

255 muscle displayed overall shorter transport distances as only 21% of the cytoplasm

256 was more than 25 µm from its nearest nucleus, increasing only slightly to 23% when

257 nuclei were randomly distributed, and 12% optimally. In spite of differences

258 between the two muscles with respect to distances within 25 µm, 98% of the

259 cytoplasm resides within a 50 µm proximity to the nearest nucleus.

260

261 **Consequences for diffusion times**

262 We here describe the differences in dimensions, distribution and density of
263 myonuclei in fibers from solus and EDL. It has however, previously been reported
264 that also the effective diffusion coefficient differs in fibers from these two muscles
265 (Papadopoulos *et al.*, 2000), and measured to be 12.5×10^{-8} cm^2s^{-1} and 18.7×10^{-8}
266 cm^2s^{-1} in soleus and EDL respectively. When combined with our data, this
267 information allows us to calculate diffusion times (t) from the nearest nuclei to any
268 point in the cell according to $t = L^2/2\sigma D$, where L is the transport distance in σ
269 dimensions, and D is the effective diffusion coefficient. The average diffusion times
270 are given for each fiber in Fig. 6 and is compared to transport times that would be
271 obtained by active transport (see Introduction).

272 We used myoglobin as an example and calculated the transportation times to each
273 point on the surface. Transport times were calculated by the geometric mean to
274 accommodate for the non-linear relationship, which causes asymmetry around the
275 mean where by few larger values of transport distances have weighted influence
276 over the diffusion times if estimated by the arithmetic mean. On average, we
277 calculated transport times to be 8.2± 1.5s and 8.4± 1.8s for EDL and soleus
278 respectively (Fig. 6A). For the diffusion times to each point in the entire cytoplasmic
279 volume, the geometric mean was 5.0± 1.3s and 5.4± 1.6s for EDL and soleus
280 respectively (Fig.6B). Thus, in spite of the large differences in dimensions, nuclear

281 density and nuclear distribution, the diffusion time was remarkably similar for the

282 two muscles.

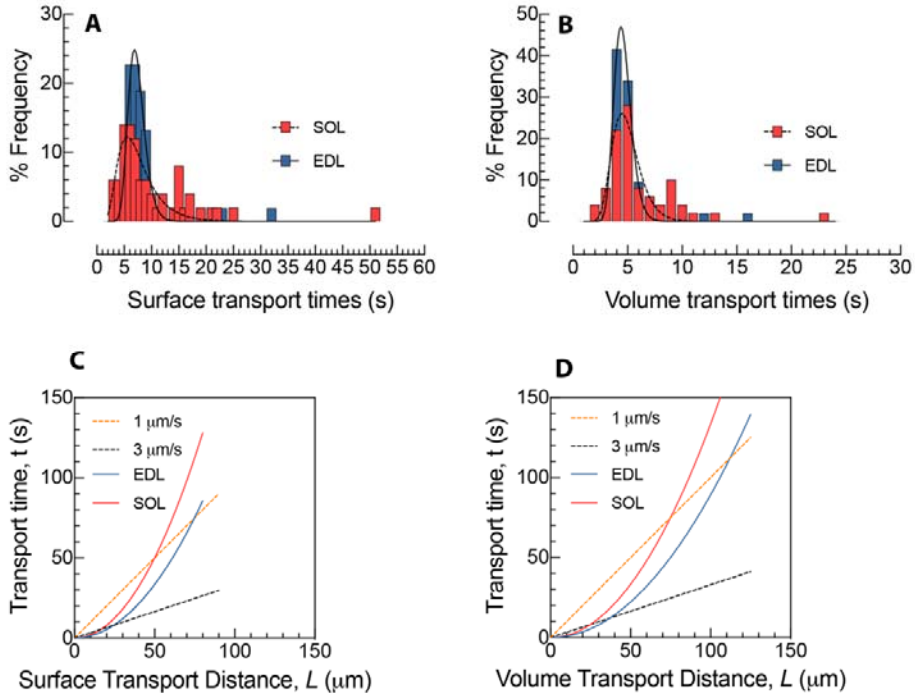

283

284 **Figure 6. EDL and soleus muscle display roughly equal diffusion times**. (A) Diffusion times plotted as the relative

285 frequency distribution versus time along the surface and within (B) fiber volume. (C) Transport times against

286 distances along the surface and (D) within the cytoplasm. Active transport at a speed of 3μm/s are highlighted by

287 dashed lines. The intersection between dashed lines and the curvilinear datapoints highlight the interface where

288 diffusion and active transport have equal transport times. At transport distances larger than the intersection,

289 active transport is faster than diffusion.

290 It is likely that intracellular transport in muscle relies both on active and passive

291 transport, but the role of active transport in muscle fibres is poorly understood.

292 Active transport along microtubules has been described in skeletal muscle (Pizon *et*

293 *al.*, 2005; Wang *et al.*, 2013) . While we are not aware of data on myosin mediated

294 transport along actin in skeletal muscle, myosin IV has been observed localized to
295 the fiber periphery, nuclei, sarcoplasmic reticulum and at the neuromuscular
296 junction (Karolczak *et al.*, 2013), and the thick-filament-associated myosin molecule
297 seems to be replaced in cultured myotubes in the absence of the microtubule
298 system (Ojima *et al.*, 2015), while the actin network per se seems to be imperative
299 for transport of membrane located molecules like e.g. the insulin sensitive glucose
300 translocator GLUT4 (Brozinick *et al.*, 2004).

301 For the transport along the surface, diffusion would be faster than actin mediated
302 transport (3μm/s) for distances of less than 15 μm in the soleus and 25 μm in the
303 EDL. When compared to transport along microtubule, diffusion would be faster for
304 distances up to 50 μm in the soleus and 75 μm in the EDL. (Fig. 6C).

305 When allowed to diffuse in three dimensions (Fig. 6D), diffusion would be faster than
306 actin mediated transport for distances of less than 24 μm in the soleus and 36 μm in
307 the EDL. When compared to transport along microtubule, diffusion would be faster
308 for distances up to 75 μm in the soleus and 112 μm in the EDL.

309

310 ## Discussion

311 We here present precise data for cell dimensions, and myonuclear density and
312 positioning in fiber segments of living muscles fibers from EDL and soleus in situ.
313 Fibers from these muscles varied with respect to all these variables, thus the radial
314 size of the EDL fibers was 31% larger than those in the soleus, while the surface or
315 volume per nuclei was 48% and 57% smaller in the soleus, respectively. In spite of
316 these differences, the transport times to points on the surface or in the cytosol are
317 remarkably similar in soleus and EDL, and we hypothesize that fibers are adapting
318 the number and positioning of nuclei in order to achieve certain transport times for
319 relevant macromolecules to all parts of the cell.

320 Given the differences in the variables related to cell dimensions and myonuclei it is a
321 paradox that the diffusion times are so similar, but is explained firstly by the
322 diffusion coefficient being 50% higher in the EDL than in the soleus, secondly, we
323 show that the nuclei are placed more optimally in the EDL. If the nuclei in the EDL
324 was placed randomly, the average surface transport distance (~27μm) versus the
325 distance observed (~23μm) would yield about 40% longer diffusion times, this would
326 translate into a 30% lower concentration of a macromolecule at any given point, and
327 the non-random positioning thus seems to be important in the EDL and cytoplasmic
328 dilution has been associated with impaired cell function in proliferative cells
329 (Miettinen & Bjorklund, 2016; Neurohr *et al.*, 2019).

330 In contrast, in the soleus the placement of nuclei appeared close to random. It is
331 possible that optimalisation of positioning is less critical since the density of nuclei is
332 higher, another explanation is that other needs override those related to internal cell
333 transport in oxidative muscles, thus in the rat soleus 81% of the nuclei appear next
334 to blood vessels (Ralston *et al.*, 2006).

335 The interior of any cell is greatly crowded by macromolecules such as ribosomes,
336 RNA and proteins (Zhou *et al.*, 2008; Smith *et al.*, 2017), which effectively reduce the
337 motion of molecules and thereby impede diffusion. Additionally, muscle fibers have
338 a dense mesh of myofibrils that occupy 80% of their total volume (van Ekeren *et al.*,
339 1992), which seems to act as exclusion zones for larger macromolecules
340 (Papadopoulos *et al.*, 2000). Taking into account the effects of macromolecular
341 crowding and scaling of transport times, it has been argued that mononuclear cells
342 have small sizes in order to optimize diffusion and signalling (Soh *et al.*, 2013). They
343 found the optimal size of a eukaryotic cell to have a radius of about 10 µm, about
344 half of the transport distance found in our calculations. This problem might be
345 aggravated, since all nuclei do not express all genes on a given time-point (Fontaine
346 & Changeux, 1989; Newlands *et al.*, 1998). Thus, the transport distances reported
347 here might represent a bottleneck limiting cell function and size of muscle fibers.

348 Disturbance of myonuclear placement impairs muscle function, e.g. after mutations
349 in the Drosophila larvae (Metzger *et al.*, 2012b; Folker & Baylies, 2013). In mammals
350 denervation which leads to grave atrophy and is accompanied by myonuclear

351 clustering eventually leaving lacunas with long transport distances (see

352 introduction). (Viguie *et al.*, 1997; Ralston *et al.*, 1999). Similarly, nuclear distribution

353 is disturbed in several myopathies and might play a causative role in impairing

354 function (Romero, 2010).

355 # Material and Methods

356 ## Animals

357 A total of 23 female NMRI mice of 20-30 grams of weight were used. The animal
358 experiments were approved by the Norwegian Animal Research Authority and were
359 conducted in accordance with the Norwegian Animal Welfare Act of 20th December
360 1974. The Norwegian Animal Research Authority provided governance to ensure
361 that facilities and experiments were in accordance with the Act, National Regulations
362 of January 15th 1996, and the European Convention for the Protection of Vertebrate
363 Animals Used for Experimental and Other Scientific Purposes of March 18th, 1986.

364 ## Preparing the mice for imaging

365 Before surgery, animals were anesthetized by a single intraperitoneal injection of a
366 zrf cocktail (18.7 mg zolazepam, 18.7 mg tiletamine, 0.45 mg xylazine and 2.6 mg
367 fentanyl per ml) that were administered at a dose of 0.08 ml per 20 g body weight.

368 The skin over the tibialis anterior and gastrocnemius was shaved and a small incision
369 was made to expose the overlaying muscles that were subsequently retracted
370 laterally to expose the EDL and soleus muscle, respectively. The epimysium was
371 gently removed, and we took care not to damage the muscle. The exposed muscle
372 was covered with a mouse Ringer's solution; NaCl 154mM, KCl 5.6 mM, $MgCl_2$ 2.2
373 mM and $NaHCO_3$ 2.4 mM, and held in place with a coverslip mounted approximately

374 2 mm above the muscle. In some muscles, the neuromuscular end plate was
375 visualized by applying Alexa 488-conjugated α-bungarotoxin (Molecular probes) to
376 the surface of the muscle for 2–3 min.

377 In vivo intracellular injections of intravital dyes were essentially done as described
378 previously (Utvik *et al.*, 1999). Animals were placed under a fixed-stage fluorescence
379 microscope (Olympus BX50WI, Olympus, Japan) with a 20X, NA 0.3, long working
380 distance water immersion objective. For *in vivo* labelling of nuclei and cytoplasm,
381 single fibers in the EDL and soleus were injected with a solution containing 5′ -
382 TRITC or FITC-labelled random 17-mer oligonucleotide with a phosphorothioated
383 backbone (Yorkshire Biosciences Ltd, Heslington, United Kingdom) and 2mg/ml
384 Cascade blue dextran (10kDa, Molecular probes) dissolved in an injection buffer (10
385 mm NaCl, 10 mm Tris, pH 7.5, 0.1 mM EDTA and 100 mM potassium gluconate) at a
386 final concentration of 0.5mM and 1mM, respectively. The oligonucleotides are taken
387 up into the nuclei inside the injected fibers probably by an active transport
388 mechanism (Hartig *et al.*, 1998), while dextran remain in the cytoplasm.

389 **Confocal Imaging**

390 Muscle fibers and nuclei in the EDL and soleus were imaged with a confocal
391 microscope (Olympus FluoView 1000, BX61W1, Olympus, Japan) in optical sections,
392 separated by z-axis steps of 1 µm to have the full three-dimensional data set of
393 nuclei. Sequential scanned fields of 0,09 mm^2 were captured, with a pixel dwell time
394 of 2µs. Movements induced by the mouse heartbeat or ventilation sometimes

395 caused displacements of individual nuclei within stacks. Therefore, mice were given
396 an overdose of the anaesthetics and image acquisition continued for 20 minutes
397 after euthanasia. No difference in myonuclear positioning and fiber morphology was
398 observed before and after euthanasia.

399 **Image analyzis**

400 In vivo images (320 x 640 pixels x 2 µm voxel depth) from optical sections of muscle
401 fibers were imported and analyzed for myonuclear number, 3D myonuclear
402 positioning, fiber volume and surface area using the Imaris bitplane 8.3.1 software
403 (Bitplane). Using the spot function in Imaris, a spot was automatically assigned to
404 each nucleus based on the fluorescence intensity from the injected oligonucleotides,
405 and if misaligned, spots were manually re-positioned to the center of each
406 myonucleus. Highlighted spots/nuclei within fibers were then given a 3D coordinate
407 in a relative Euclidean space using the Imaris Vantage extension. Volume and surface
408 rendering were performed using the fluorescence from Cascade blue conjugated
409 dextran in the cytoplasm. Rendering of fiber volume was performed using the
410 fluorescence perimeter border of the fiber in the cross-sectional direction as an
411 outer limit, and thereby preserving fiber morphology during quantification.

Computer modelling of nuclear distribution

Once the Euclidian coordinates of the myonuclei were obtained in Imaris, fiber surfaces were approximated by fitting the points to the surface of an idealized elliptical cylinder surface.

An elliptical cylinder oriented along the *z*-axis, with its major and minor axes oriented along the *x*- and *y*-axes, respectively, can be parameterized as

$$\frac{(x-x_0)^2}{a^2} + \frac{(y-y_0)^2}{b^2} = 1,$$

where a and b are the major and minor axes, respectively, and is the point where the center of the cylinder intercepts the *xy*-plane.

The cylinder was parameterized by the Euler angles pointing along the z-axis of the cylinder, the major and minor axes of the ellipse, the angle of the major axis relative to the x-axis, and the x- and y-coordinates of the center of the ellipse, for a total of 8 free variables. The optimization was carried out in two rounds, where the Euler angles were chosen first, after which the remaining ellipse fitting was completed for the given angles, using a direct least squares fitting. The angles were then updated using MATLABs interior point optimization solver, until convergence was achieved.

Subsequently, the 3-dimensional coordinates of the nuclei retrieved form Imaris were mapped to the 2-dimensional coordinates consisting of the position along the

431 z-axis and distance along the ellipse circumference relative to the major axis. Next,
432 we calculated area and volumes defined by Voronoi geometries of each nucleus and
433 distance maps for all points on the cylinder surface to the nearest nuclei, based on
434 the distance along the cylinder surface, noting that the surface is periodic along the
435 circumference.

436 Additionally, we ran Monte Carlo simulations and nuclei were randomly placed on
437 the parameterized surface in order to compare the distance map to that of the
438 observed fibers. By a Lloyd's Algorithm, we also placed the nuclei optimally on the
439 surface, such that the Voronoi domains for all nuclei were equal and compared it to
440 an observed distribution of nuclear patterns.

441 All codes used in the computational modelling can be found at
442 https://github.com/CINPLA/cylinderTools.

443 **Statistics**

444 Data were derived from 53 fibers injected on the lateral surface of EDL (N=9 animals)
445 and 51 fibers injected at dorsal surface of the soleus muscle (N=12 animals).
446 Descriptive statistics are shown as the pooled sum of fibers for a given muscle. If not
447 stated otherwise, numbers are presented as mean± standard deviation (mean± SD).
448 Frequently, point pattern analysis, including Voronoi segmentation, subdivide the
449 area or volume of interest into a subset of polygons (2D) or polyhedrons (3D). In
450 Voronoi segmentation, the number of Voronoi polygons is proportional to number of
451 points in the plane or room. In our case, the number of points is equal to the nuclear

452 number within each muscle fiber. Thus, if an area (or volume) is divided into the
453 same number of domain objects, the average size of objects remains the same in
454 spite of differences in the nuclear patterning (i.e. because the total area, volume and
455 number of points are unchanged). Instead, we used the variation (standard
456 deviation) as a measure of similarity between the observed mean size of polygons,
457 to those when nuclei were placed randomly or optimally. We statistically compared
458 standard deviations of domain areas and domain volumes by differences in nuclear
459 patterning by a one-way ANOVA followed by a Tukey's correction for multiple
460 comparisons.

461 In comparison, we are not faced with the same problem as outlined for the Voronoi
462 segmentation when analyzing transport distances between different nuclear
463 distributions. They were therefore analyzed statistically by a Brown-Forsythe analysis
464 followed by a Games-Howell's multiple comparisons test at a 5 % significance level.

465 All graphs and statistical analyzis were plotted and performed in Prism 8 (Graphpad).
466

467 **References**

468 Brozinick JT, Jr., Hawkins ED, Strawbridge AB & Elmendorf JS. (2004). Disruption
469 of cortical actin in skeletal muscle demonstrates an essential role of the
470 cytoskeleton in glucose transporter 4 translocation in insulin-sensitive
471 tissues. *J Biol Chem* **279,** 40699-40706.

472 Bruusgaard JC, Liestol K, Ekmark M, Kollstad K & Gundersen K. (2003). Number
473 and spatial distribution of nuclei in the muscle fibres of normal mice
474 studied in vivo. *J Physiol* **551,** 467-478.

475 Bruusgaard JC, Liestol K & Gundersen K. (2006). Distribution of myonuclei and
476 microtubules in live muscle fibers of young, middle-aged, and old mice. *J*
477 *Appl Physiol (1985)* **100,** 2024-2030.

478 Cadart C, Venkova L, Recho P, Lagomarsino MC & Piel M. (2019). The physics of
479 cell-size regulation across timescales. *Nat Phys* **15,** 993-1004.

480 Cheek DB. (1985). The control of cell mass and replication. The DNA unit--a
481 personal 20-year study. *Early Hum Dev* **12,** 211-239.

482 Cristea A, Qaisar R, Edlund PK, Lindblad J, Bengtsson E & Larsson L. (2010).
483 Effects of aging and gender on the spatial organization of nuclei in single
484 human skeletal muscle cells. *Aging Cell* **9,** 685-697.

485 Du Q, Gunzburger M & Ju LL. (2010). Advances in Studies and Applications of
486 Centroidal Voronoi Tessellations. *Numer Math-Theory Me* **3,** 119-142.

487 Folker ES & Baylies MK. (2013). Nuclear positioning in muscle development and
488 disease. *Front Physiol* **4,** 363.

489 Fontaine B & Changeux JP. (1989). Localization of nicotinic acetylcholine
490 receptor a-subunit transcripts during myogenesis and motor endplate
491 development in the chick. *J Cell Biol* **108,** 1025-1037.

492 Frair PM & Peterson AC. (1983). The nuclear-cytoplasmic relationship in 'mosaic'
493 skeletal muscle fibers from mouse chimaeras. *Exp Cell Res* **145,** 167-178.

494 Gundersen K. (2016). Muscle memory and a new cellular model for muscle
495 atrophy and hypertrophy. *J Exp Biol* **219,** 235-242.

496 Gundersen K & Merlie JP. (1993). Regulation of nicotinic acetyl choline receptor
497 genes by overexpressing myogenin and Id in transgenic mice. *Society for*
498 *Neuroscience Abstracts* **19,** 223.

499

500 Hall ZW & Ralston E. (1989). Nuclear domains in muscle cells. *Cell* **59,** 771-772.

501 Hartig R, Shoeman RL, Janetzko A, Grüb S & Traub P. (1998). Active nuclear
502 import of singel-stranded oligonucleotides and their complexes with non-
503 karyophilic macromolcules. *Biology og the Cell* **90,** 407-426.

504 Kann F. (1957). [Diameter and number of muscle fibers in various cross section
505 levels of sartorius muscle in man]. *Acta Anat (Basel)* **30,** 351-357.

506 Karolczak J, Sobczak M, Majewski L, Yeghiazaryan M, Jakubiec-Puka A, Ehler E,
507 Slawinska U, Wilczynski GM & Redowicz MJ. (2013). Myosin VI in skeletal
508 muscle: its localization in the sarcoplasmic reticulum, neuromuscular
509 junction and muscle nuclei. *Histochem Cell Biol* **139,** 873-885.

510 Merlie JP, Isenberg KE, Russell SD & Sanes JR. (1984). Denervation
511 supersensitivity in skeletal muscle: analysis with a cloned cDNA probe. *J*
512 *Cell Biol* **99,** 332-335.

513 Merlie JP & Sanes JR. (1985). Concentration of acetylcholine receptor mRNA in
514 synaptic regions of adult muscle fibres. *Nature* **317,** 66-68.

515 Metzger T, Gache V, Xu M, Cadot B, Folker E, Richardson BE, Gomes ER & Baylies
516 MK. (2012a). MAP and kinesin-dependent nuclear positioning is required
517 for skeletal muscle function. *Nature* **484,** 120.

518 Metzger T, Gache V, Xu M, Cadot B, Folker ES, Richardson BE, Gomes ER & Baylies
519 MK. (2012b). MAP and kinesin-dependent nuclear positioning is required
520 for skeletal muscle function. *Nature* **484,** 120-124.

521 Miettinen TP & Bjorklund M. (2016). Cellular Allometry of Mitochondrial
522 Functionality Establishes the Optimal Cell Size. *Dev Cell* **39,** 370-382.

523 Mintz B & Baker WW. (1967). Normal mammalian muscle differentiation and
524 gene control of isocitrate dehydrogenase synthesis. *Proc Natl Acad Sci U S*
525 *A* **58,** 592-598.

526 Mishra P, Varuzhanyan G, Pham AH & Chan DC. (2015). Mitochondrial Dynamics
527 is a Distinguishing Feature of Skeletal Muscle Fiber Types and Regulates
528 Organellar Compartmentalization. *Cell Metab* **22,** 1033-1044.

529 Neurohr GE, Terry RL, Lengefeld J, Bonney M, Brittingham GP, Moretto F,
530 Miettinen TP, Vaites LP, Soares LM, Paulo JA, Harper JW, Buratowski S,
531 Manalis S, van Werven FJ, Holt LJ & Amon A. (2019). Excessive Cell
532 Growth Causes Cytoplasm Dilution And Contributes to Senescence. *Cell*
533 **176,** 1083-1097 e1018.

534

535 Nevalainen M, Kaakinen M & Metsikko K. (2013). Distribution of mRNA
536 transcripts and translation activity in skeletal myofibers. *Cell Tissue Res*
537 **353,** 539-548.

538 Newlands S, Levitt LK, Robinson CS, Karpf AB, Hodgson VR, Wade RP &
539 Hardeman EC. (1998). Transcription occurs in pulses in muscle fibers.
540 *Genes Dev* **12,** 2748-2758.

541 Ojima K, Ichimura E, Yasukawa Y, Wakamatsu J & Nishimura T. (2015). Dynamics
542 of myosin replacement in skeletal muscle cells. *Am J Physiol Cell Physiol*
543 **309,** C669-679.

544 Papadopoulos S, Jurgens KD & Gros G. (2000). Protein diffusion in living skeletal
545 muscle fibers: dependence on protein size, fiber type, and contraction.
546 *Biophys J* **79,** 2084-2094.

547 Pavlath GK, Rich K, Webster SG & Blau HM. (1989). Localization of muscle gene
548 products in nuclear domains. *Nature* **337,** 570-573.

549 Pilling AD, Horiuchi D, Lively CM & Saxton WM. (2006). Kinesin-1 and Dynein are
550 the primary motors for fast transport of mitochondria in Drosophila
551 motor axons. *Mol Biol Cell* **17,** 2057-2068.

552 Pizon V, Gerbal F, Diaz CC & Karsenti E. (2005). Microtubule-dependent
553 transport and organization of sarcomeric myosin during skeletal muscle
554 differentiation. *EMBO J* **24,** 3781-3792.

555 Ralston E & Hall ZW. (1992a). Restricted distribution of mRNA produced from a
556 single nucleus in hybrid myotubes. *JCB* **119,** 1063-1068.

557 Ralston E & Hall ZW. (1992b). Restricted distribution of mRNA produced from a
558 single nucleus in hybrid myotubes. *J Cell Biol* **119,** 1063-1068.

559 Ralston E, Lu Z, Biscocho N, Soumaka E, Mavroidis M, Prats C, Lomo T,
560 Capetanaki Y & Ploug T. (2006). Blood vessels and desmin control the
561 positioning of nuclei in skeletal muscle fibers. *J Cell Physiol* **209,** 874-882.

562 Ralston E, Lu Z & Ploug T. (1999). The organization of the Golgi complex and
563 microtubules in skeletal muscle is fiber type-dependent. *J Neurosci* **19,**
564 10694-10705.

565 Romero NB. (2010). Centronuclear myopathies: a widening concept.
566 *Neuromuscul Disord* **20,** 223-228.

567 Sandve GK, Gundersen S, Rydbeck H, Glad IK, Holden L, Holden M, Liestol K,
568 Clancy T, Drablos F, Ferkingstad E, Johansen M, Nygaard V, Tostesen E,
569 Frigessi A & Hovig E. (2011). The differential disease regulome. *BMC*
570 *genomics* **12,** 353.

571 Sanes JR, Johnson YR, Kotzbauer PT, Mudd J, Hanley T, Martinou JC & Merlie JP.
572 (1991). Selective expression of an acetylcholine receptor-lacZ transgene
573 in synaptic nuclei of adult muscle fibres. *Dev* **113,** 1181-1191.

574 Schott DH, Collins RN & Bretscher A. (2002). Secretory vesicle transport velocity
575 in living cells depends on the myosin-V lever arm length. *J Cell Biol* **156,**
576 35-39.

577 Smith S, Cianci C & Grima R. (2017). Macromolecular crowding directs the
578 motion of small molecules inside cells. *J R Soc Interface* **14**.

579 Soh S, Banaszak M, Kandere-Grzybowska K & Grzybowski BA. (2013). Why Cells
580 are Microscopic: A Transport-Time Perspective. *J Phys Chem Lett* **4,** 861-
581 865.

582 Strassburger E. (1893). Ûber die Wirkungssphäre der kerne und die zellgrösse.
583 *Histol Beitr* **5,** 97-124.

584 Utvik JK, Nja A & Gundersen K. (1999). DNA injection into single cells of intact
585 mice. *Hum Gene Ther* **10,** 291-300.

586 van Ekeren GJ, Sengers RC & Stadhouders AM. (1992). Changes in volume
587 densities and distribution of mitochondria in rat skeletal muscle after
588 chronic hypoxia. *Int J Exp Pathol* **73,** 51-60.

589 Viguie CA, Lu DX, Huang SK, Rengen H & Carlson BM. (1997). Quantitative study
590 of the effects of long-term denervation on the extensor digitorum longus
591 muscle of the rat. *Anat Rec* **248,** 346-354.

592 Wang Z, Cui J, Wong WM, Li X, Xue W, Lin R, Wang J, Wang P, Tanner JA, Cheah
593 KS, Wu W & Huang JD. (2013). Kif5b controls the localization of myofibril
594 components for their assembly and linkage to the myotendinous
595 junctions. *Development* **140,** 617-626.

596 Zhou HX, Rivas G & Minton AP. (2008). Macromolecular crowding and
597 confinement: biochemical, biophysical, and potential physiological
598 consequences. *Annu Rev Biophys* **37,** 375-397.

599

600